

Nonlinear Dendritic Coincidence Detection for Supervised Learning

Fabian Schubert^{1,*} and Claudius Gros¹

¹*Institute for Theoretical Physics, Goethe University Frankfurt am Main, Germany*

Correspondence*:

Institute for Theoretical Physics
Goethe University Frankfurt am Main
Max-von-Laue-Str. 1
60438 Frankfurt am Main, Germany
fschubert@itp.uni-frankfurt.de

2 ABSTRACT

3 Cortical pyramidal neurons have a complex dendritic anatomy, whose function is an active field
4 of scientific research. In particular, the segregation between its soma and the apical dendritic tree
5 is believed to play an active role in processing feed-forward sensory information and top-down
6 or feedback signals. In this work, we use a simple two-compartment model accounting for the
7 nonlinear interactions between basal and apical input streams and show that a simple Hebbian
8 learning rule in the basal compartment allows the neuron to align its basal input to a target
9 signal in the apical compartment. We show that this learning process is robust against strong
10 distractions in the basal input space and demonstrate its effectiveness in a linear classification
11 task.

12 **Keywords:** Dendrites, Pyramidal Neuron, Plasticity, Coincidence Detection, Supervised Learning

1 INTRODUCTION

13 In recent years, a growing body of research has addressed the functional implications of the distinct
14 physiology and anatomy of cortical pyramidal neurons Spruston (2008); Hay et al. (2011); Ramaswamy
15 and Markram (2015). In particular, on the theoretical side, we saw a paradigm shift from treating neurons
16 as point-like electrical structures towards embracing the entire dendritic structure Larkum et al. (2009);
17 Poirazi (2009); Shai et al. (2015a). This was mostly due to the fact that experimental work uncovered
18 dynamical properties of these cells that simply could not be accounted for by point models Spruston et al.
19 (1995); Häusser et al. (2000).

20 An important finding was that the apical dendritic tree of cortical pyramidal neurons can act as a separate
21 nonlinear synaptic integration zone Spruston (2008); Branco and Häusser (2011). Under certain conditions,
22 a dendritic Ca^{2+} spike can be elicited that propagates towards the soma, causing rapid, bursting spiking
23 activity. One of the cases in which dendritic spiking can occur was termed ‘backpropagation-activated Ca^{2+}
24 spike firing’ (‘BAC firing’): A single somatic spike can backpropagate towards the apical spike initiation
25 zone, in turn significantly facilitating the initiation of a dendritic spike Stuart and Häusser (2001); Spruston
26 (2008); Larkum (2013). This reciprocal coupling is believed to act as a form of coincidence detection: If
27 apical and basal synaptic input co-occurs, the neuron can respond with a rapid burst of spiking activity.
28 The firing rate of these temporal bursts exceeds the firing rate that is maximally achievable under basal

synaptic input alone, therefore representing a form of temporal coincidence detection between apical and basal input.

Naturally, these mechanisms also affect plasticity and thus learning within the cortex Sjöström and Häusser (2006); Ebner et al. (2019). While the interplay between basal and apical stimulation and its effect on synaptic efficacies is subject to ongoing research, there is some evidence that BAC-firing tends to shift plasticity towards long-term potentiation (LTP) Letzkus et al. (2006). Thus, coincidence between basal and apical input appears to also gate synaptic plasticity.

In a supervised learning scheme, where the top down input arriving at the apical compartment acts as the teaching signal, the most straight-forward learning rule for the basal synaptic weights would be derived from an appropriate loss function, such as a mean square error, based on the difference between basal and apical input, i.e. $I_p - I_d$. Theoretical work has investigated possible learning mechanisms that could utilize an intracellular error signal (Urbanczik and Senn, 2014; Schiess et al., 2016; Guerguiev et al., 2017). However, a clear experimental evidence for a physical quantity encoding such an error is—to our knowledge—yet to be found. On the other hand, Hebbian-type plasticity is extensively documented in experiments Gustafsson et al. (1987); Debanne et al. (1994); Markram et al. (1997); Bi and Poo (1998). Therefore, our work is based on the question whether the non-linear interactions between basal and apical synaptic input could, when combined with a Hebbian plasticity rule, allow a neuron to learn to reproduce an apical teaching signal in its proximal input.

In our work, we combine a phenomenological model that generates the output firing rate as a function of two streams of synaptic input (subsuming basal and apical input) with Hebbian, as well as BCM-like plasticity rules on basal synapses. We hypothesized that this combination of neural activation and plasticity rules would lead to an increased correlation between basal and apical input.

Furthermore, this temporal alignment could potentially facilitate apical inputs to act as top-down teaching signals, without the need for an explicit error-driven learning rule. Thus, we also test our model in a simple linear supervised classification task and compare it with the performance of a simple point neuron equipped with similar plasticity rules.

2 MODEL

2.1 Neuron Model

The neuron model used throughout this study is a discrete-time rate encoding model that uses two separate input variables, subsuming the total synaptic input current injected arriving at the basal (proximal) and apical (distal) dendritic structure of a pyramidal neuron, respectively. The model is a slightly simplified version of a phenomenological model proposed by Shai et al. (2015b). Denoting the input currents I_p (proximal) and I_d (distal), the model is written as

$$y(t) = \alpha \sigma(I_p(t) - \theta_{p0}) [1 - \sigma(I_d(t) - \theta_d)] + \sigma(I_d(t) - \theta_d) \sigma(I_p(t) - \theta_{p1}) \quad (1)$$

$$\sigma(x) \equiv \frac{1}{1 + \exp(-4x)} . \quad (2)$$

Here, θ_{p0} , θ_{p1} and θ_d are threshold variables with respect to proximal and distal input. Overall, this equation describes two distinct regions of neural activation in the (I_p, I_d) -space which differ in their maximal firing rates, which are set to 1 and α , where $0 < \alpha < 1$. A plot of (1) is shown in Fig. 1.

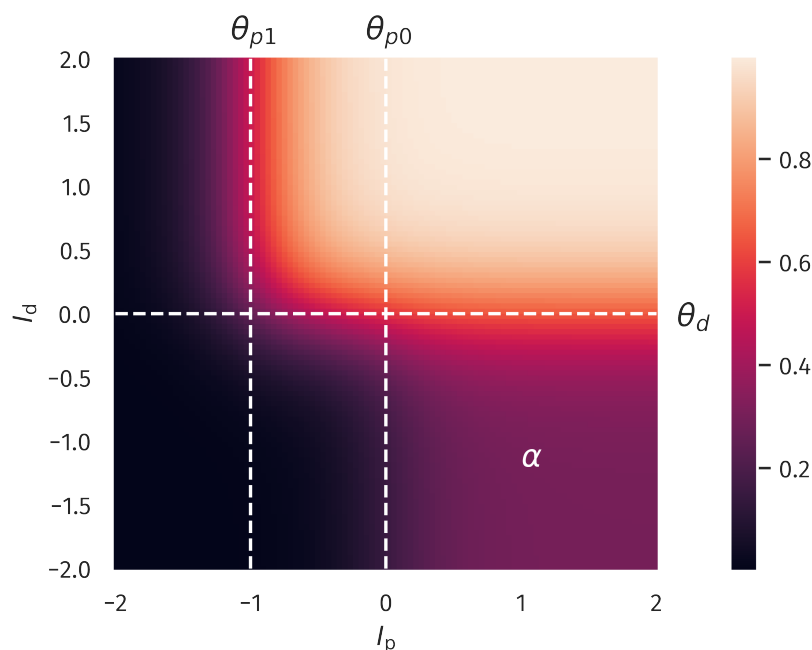


Figure 1. Two-compartment rate model. Firing rate as a function of proximal and distal input I_p and I_d , see (1). The thresholds θ_{p0} , θ_{p1} and θ_d define two regions of neural activity with a maximal firing rate of 1 and α .

In all our numerical experiments, we compare this model with a simple point neuron model that was given by

$$y(t) = \sigma(I_p(t) + I_d(t) - \theta) . \quad (3)$$

The apical input I_d was generated ‘as is’, meaning, it is not dynamically calculated as a superposition of multiple presynaptic inputs, but given by

$$I_d(t) = n_d(t)x_d(t) - b_d(t) , \quad (4)$$

where $n_d(t)$ is a scaling factor, $x_d(t)$ a pre-generated discrete time sequence and $b_d(t)$ a bias. Note that n_d and b_d are time dependent since they are subject to adaptation processes that are described in the next section.

Similarly, $I_p(t)$ is given by

$$I_p(t) = n_p(t) \sum_{i=1}^N x_{p,i}(t)w_i(t) - b_p(t) , \quad (5)$$

where N is the number of presynaptic afferents, $x_{p,i}(t)$ the corresponding sequences and $w_i(t)$ the synaptic efficacies. As for $I_d(t)$, $n_p(t)$ and $b_p(t)$ is a time dependent scaling and bias.

θ_{p0}	0	V_d^t	0.25
θ_{p1}	-1	μ_b	10^{-3}
θ_d	0	μ_n	10^{-4}
α	0.3	μ_{av}	$5 \cdot 10^{-3}$
μ_w	$5 \cdot 10^{-5}$	I_p^t	0
V_p^t	0.25	I_d^t	0

Table 1. Model parameters

69 2.2 Plasticity

We implemented a Hebbian plasticity rule for the basal synaptic weights given by the following update equation:

$$w_i(t+1) = w_i(t) + \mu_w (x_{p,i}(t) - \tilde{x}_{p,i}(t)) (y(t) - \tilde{y}) \quad (6)$$

$$\tilde{x}_{p,i}(t+1) = (1 - \mu_{av})\tilde{x}_{p,i}(t) + \mu_{av}x_{p,i}(t+1) \quad (7)$$

$$\tilde{y}(t+1) = (1 - \mu_{av})\tilde{y}(t) + \mu_{av}y(t+1) \quad (8)$$

70 Additionally, we use a synaptic normalization constraint

$$w_i(t) \rightarrow \frac{w_i(t)}{\|\mathbf{w}(t)\|} \quad (9)$$

71 in each time step, where $\|\mathbf{w}(t)\|$ denotes the Euclidean norm of the synaptic weight vector.

72 For comparative reasons, the point neuron model is equipped with the same plasticity rule for the proximal
73 weights as (6).

Additionally, the scaling and bias variables are changing dynamically according to the following homeostatic plasticity rules:

$$b_p(t+1) = b_p(t) + \mu_b [I_p(t) - I_p^t] \quad (10)$$

$$b_d(t+1) = b_d(t) + \mu_b [I_d(t) - I_d^t] \quad (11)$$

$$n_p(t+1) = n_p(t) + \mu_n \left[V_p^t - \left(I_p(t) - \tilde{I}_p(t) \right)^2 \right] \quad (12)$$

$$n_d(t+1) = n_d(t) + \mu_n \left[V_d^t - \left(I_d(t) - \tilde{I}_d(t) \right)^2 \right] \quad (13)$$

$$\tilde{I}_p(t+1) = (1 - \mu_{av})\tilde{I}_p(t) + \mu_{av}I_p(t+1) \quad (14)$$

$$\tilde{I}_d(t+1) = (1 - \mu_{av})\tilde{I}_d(t) + \mu_{av}I_d(t+1) \quad (15)$$

74 Here, I_p^t , I_d^t , V_p^t and V_d^t define targets for the temporal means and variances of I_p and I_d . The dynamic
75 variables \tilde{I}_p and \tilde{I}_d are simply low-pass filtered running averages of I_p and I_d .

76 A list of all parameter values is given in Table 1.

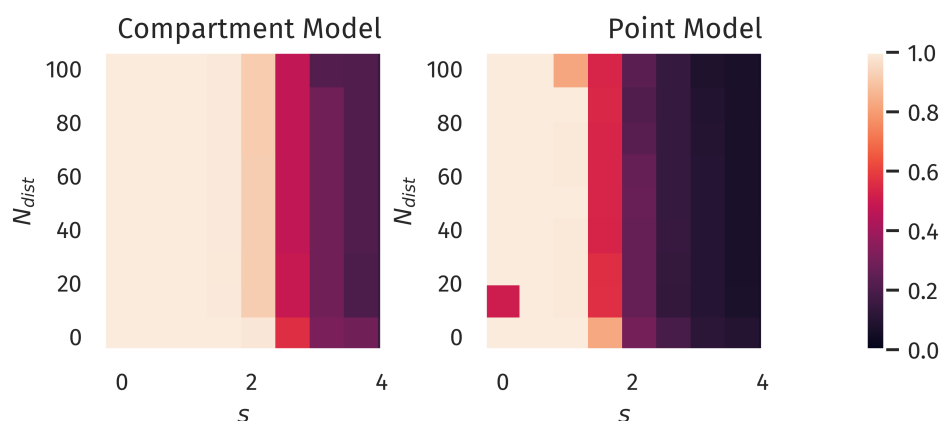


Figure 2. Alignment between Basal and Apical Input. Color encodes the Pearson correlation $\rho[I_p, I_d]$ for different number of orthogonal distraction directions N_{dist} and the corresponding scaling factor s .

3 RESULTS

3.1 Increased Alignment between Basal and Apical Inputs

As a first test, we wanted to quantify the neuron's ability to align its basal input to the apical teaching signal. To do so, we defined the pearson correlation coefficient $\rho[I_p, I_d]$ between the basal and apical input current as our measure of interest. We determined this temporal correlation coefficient after simulating all plasticity mechanisms under stationary random input sequences with certain statistical properties that shall be explained in the following. As a starting point, we chose all $x_{p,i}(t)$ to be randomly drawn from a uniform distribution, where $x_{p,i}(t) \in (0, 1)$. For $I_d(t)$ to be fully 'reconstructable' by the basal input, $x_d(t)$ had to be some linear combination of all $x_{p,i}(t)$. Therefore, we chose $x_d(t) = \sum_{i=1}^N a_i x_{p,i}(t)$, where \mathbf{a} is a random vector with unit length. Since we used a Hebbian learning scheme, we expected that the direction and magnitude of the principal components of the basal input would also significantly affect the outcome of the experiment: A large variance in the basal input orthogonal to the 'reconstruction vector' \mathbf{a} should act as a distraction for the plasticity and reduce the resulting alignment between I_p and I_d . Therefore, we applied a transformation to the input sequences $x_{p,i}(t)$ that were parameterized by two quantities, a scaling factor s and the dimension N_{dist} of a subspace of the basal input space. A set of N_{dist} orthonormal basis vectors was randomly generated, which were also orthogonal to \mathbf{a} . Withing this N_{dist} -dimensional subspace, the input sequences $x_{p,i}(t)$ were then rescaled by the factor s .

After both $x_{p,i}(t)$ and $x_d(t)$ were generated, a simulation was run using all previously described plasticity mechanisms until the dynamic variables reached a stationary state. After this learning phase, another set of input sequences was generated using the previously described protocol and $\rho[I_p, I_d]$ was calculated. Note that plasticity was turned off in this phase. This entire procedure allowed us to calculate $\rho[I_p, I_d]$ as a function of the distraction parameters s and N_{dist} . The results for both neuron models is shown in Fig. 2. Here, the total number of basal inputs is $N = 10$. One can observe a decorrelation transition for both models. However, the compartment model supports a significantly stronger distraction in terms of the scaling factor s as compared to the point model. This is a first confirmation of our hypothesis that nonlinear interactions between basal and apical input could improve learning guided by top-down signals.

3.2 Supervised Learning in a Linear Classification Task

Next, we investigated if the observed differences would also improve the performance in an actual supervised learning task. For this purpose, we constructed presynaptic basal input as illustrated in Fig. 3.

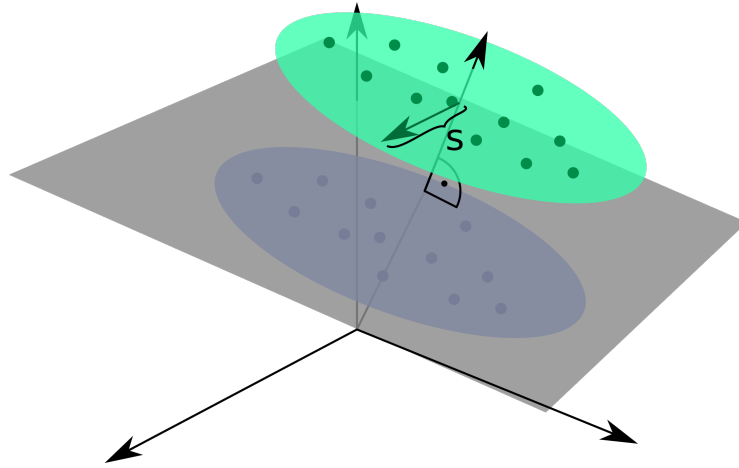


Figure 3. Input Space for a Simple Linear Classification Task. Two clusters of presynaptic basal activity were generated from multivariate Gaussian distributions. Here, s denotes the standard deviation orthogonal to the normal vector of the classification hyperplane.

105 Written in vector form, each sample from the basal input is generated from the following expression:

$$\mathbf{x}_p(t) = \mathbf{b} + \mathbf{a} (c(t) + \sigma_a \zeta_a(t)) + s \cdot \sum_{i=1}^{N_{dist}} \zeta_{dist,i}(t) \mathbf{v}_{dist,i} . \quad (16)$$

Here, \mathbf{b} is a random vector drawn uniformly from $(0, 1)^N$, \mathbf{a} is random unit vector as introduced in Section 3.1, $c(t)$ is a binary variable drawn from $\{-0.5, 0.5\}$ with equal probability and $\zeta_a(t)$ and the $\zeta_{dist,i}(t)$ are independent random Gaussian variables with zero mean and unit variance. Hence, σ_a simply denotes the standard deviation of each Gaussian cluster along the direction of the normal vector \mathbf{a} and was set to $\sigma_a = 0.25$. Finally, the set of $\mathbf{v}_{dist,i}$ forms a randomly generated orthogonal basis of N_{dist} unit vectors which—just as in Section 3.1—are also orthogonal to \mathbf{a} . The free parameter s parameterized the standard deviation along this subspace orthogonal to \mathbf{a} . As indicated by the time dependence, the Gaussian and binary random variables are drawn for each time step. The vectors \mathbf{b} , \mathbf{a} , and $\mathbf{v}_{dist,i}$ are generated once before the beginning of a simulation run. For the classification task, we set up two output neurons receiving the same basal presynaptic input, while the top-down input encoded the correct linear classification in a one-hot scheme, that is

$$x_{d,0}(t) = 1 - \Theta \left((\mathbf{x}_p(t) - \mathbf{b})^T \mathbf{a} \right) \quad (17)$$

$$x_{d,1}(t) = \Theta \left((\mathbf{x}_p(t) - \mathbf{b})^T \mathbf{a} \right) , \quad (18)$$

106 where $\Theta(x)$ is the Heaviside step function.

107 As in the previous experiment, we ran a full simulation until all dynamic variables reached a stationary
 108 state. After this, a test run without plasticity and with the apical input turned off was used to evaluate the
 109 classification performance. For each sample, the index of the neuron with the highest activity was used as
 110 the predicted class. Accuracy was then calculated as the fraction of correctly classified samples.

111 The resulting accuracy as a function of N_{dist} and s is shown in Fig. 4. Albeit differences are small, the
 112 compartment model does show a better overall accuracy for the tested parameter range. It should be noted,

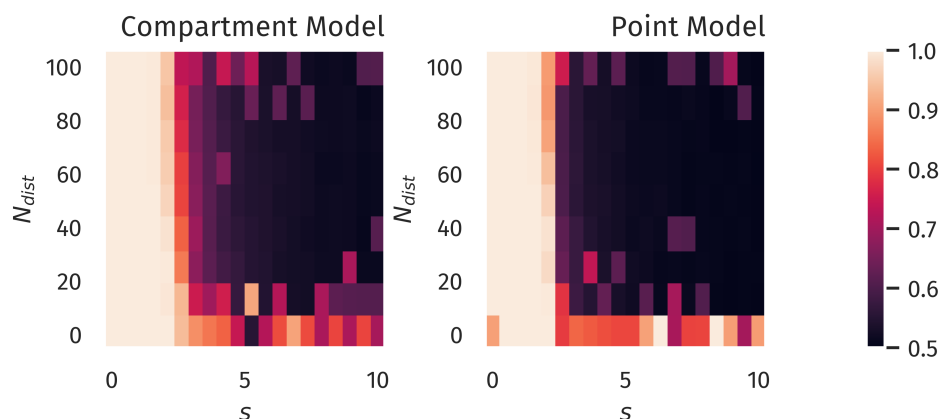


Figure 4. Binary Classification Accuracy. Fraction of correctly classified patterns as illustrated in Fig. 3, see Section 3.2.,

though, that the advantage of the compartment model becomes even less prominent when looking at the actual correlation between proximal and distal input as a measure of successful learning (as done in the previous section). Fig. 8 in the supplementary section shows that the compartment model allows for a marginally larger scaling among the distraction dimensions.

3.3 Non-Hebbian Learning Rules

Instead of Hebbian learning, we also considered a BCM-like learning rule for the basal weights (Bienenstock et al., 1982; Intrator and Cooper, 1992). The form of the BCM-rule we consider here reads

$$\Delta w_i \propto y(y - \theta_M)x_i - \epsilon w_i, \quad (19)$$

where θ_M is a threshold defining a transition from LTP to LTD and ϵ is an optional decay term on the weights. In the variant introduced by Law and Cooper (1994), the sliding threshold is simply the temporal average of the squared neural activity, $\theta_M = \langle y^2 \rangle$. In practice, this would be calculated as a running average, thereby preventing the weights from growing indefinitely.

However, for our compartment model, we chose to explicitly set the threshold to be the mean value between the high- and low-activity regime in our compartment model, i.e. $\theta_M = (1 + \alpha)/2$. By doing so, LTP is preferably induced if both basal and apical input are present at the same time. Furthermore, instead of the weight decay term, we chose to keep the weight normalization as introduced in (9). Obviously, for the point model, the reasoning behind our choice of θ_M did not apply. Still, to provide some level of comparability, we also ran simulations with a point model where the sliding threshold was calculated as a running average of y^2 . Furthermore, we did not use weight normalization in this case, but chose to use a small weight decay term with $\epsilon = 0.1$. The results are shown in Fig. 5 (classification task) and Fig. 5 (Basal-Apical alignment). While the accuracy of the classification for the point model is at most comparable to Hebbian learning, the BCM-like rule for the compartment model significantly increases the accuracy for the tested parameter range (compare Fig. 4). Still, as for the Hebbian learning rule, this result should be taken with a grain of salt, as Fig. 9 in the supplementary section indicates that a rather large part of the region ($s > 5$) showing good classification performance for the compartment model in Fig. 5 does hardly exhibit any actual correlation between proximal and distal input, making it likely that the accuracy of the classification could be easily impaired in this regime, e.g. by injecting small amounts of noise.

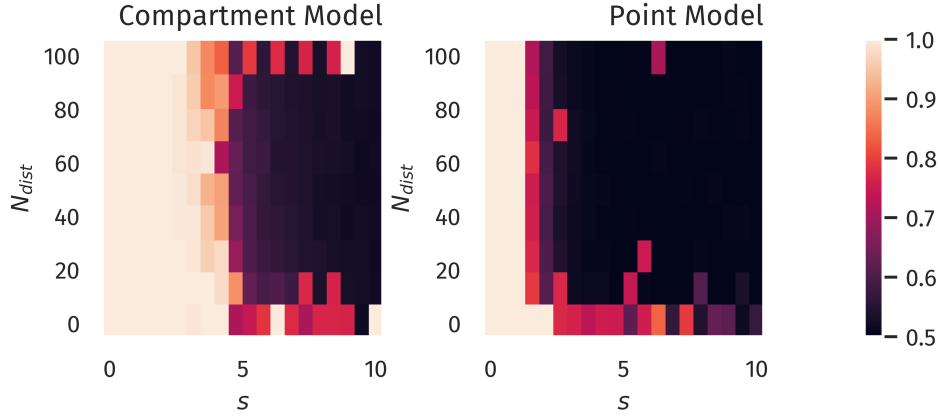


Figure 5. Binary Classification Accuracy, BCM Rule. Fraction of correctly classified patterns as illustrated in Fig. 3, after training with a BCM-like learning rule.

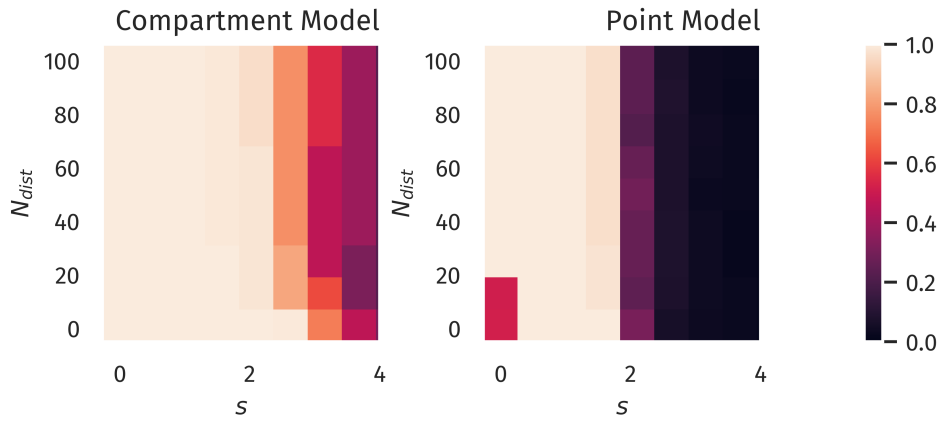


Figure 6. Alignment between Basal and Apical Input, BCM Rule. Color encodes the Pearson correlation $\rho[I_p, I_d]$ for different number of orthogonal distraction directions N_{dist} and the corresponding scaling factor s after training with a BCM-like rule. Compare to Fig. 2.

141 The compartment model also significantly benefits from the BCM rule in terms of basal-apical alignment
 142 as tested in Sect. 3.1, while only marginal improvements can be observed for the point model (compare
 143 Fig. 6 with Fig. 2).

144

145 3.4 Objective Function of BCM Learning in the Compartment Model

147 To form a better understanding of why the BCM-type learning rule in combination with the implemented
 148 compartment model, we can formalize the learning rule for the proximal weights in terms of an objective
 149 function. For this purpose, we further simplify (1) by replacing the sigmoid functions $\sigma(x)$ by a simple step
 150 function $\Theta(x)$. This does not change the overall shape or topology of the activation in the (I_p, I_d) space
 151 but merely makes the smooth transitions sharp and instantaneous. Using $\Delta w_i \propto y(y - \theta_M)x_i$, we find in
 152 this case

$$\begin{aligned} \Delta w_i \propto & [(1 - \alpha)\Theta(I_d - \theta_d)\Theta(p - \theta_{p1}) \\ & + \alpha(\alpha - 1)\Theta(\theta_d - I_d)\Theta(p - \theta_{p0})]x_i. \end{aligned} \quad (20)$$

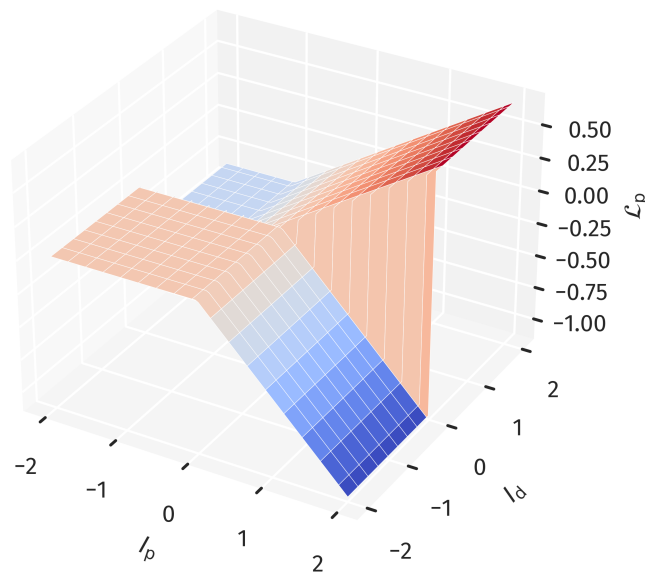


Figure 7. Objective Function for the Proximal Weight Update. The approximate objective function for the proximal weights as given in (22). This corresponds to a combination of using (1) together with (19). Note the ridge-like structure along the I_p - I_d diagonal, which supports the alignment between proximal and distal input.

Noting that $\Theta(x)$ is the first derivative of the ReLu function $[x]^+ \equiv \max(0, x)$, we find that this update rule can be written as

$$\Delta w_i \propto \frac{\partial \mathcal{L}_p}{\partial w_i} \quad (21)$$

$$\begin{aligned} \mathcal{L}_p \equiv & (1 - \alpha)\Theta(I_d - \theta_d)[p - \theta_{p1}]^+ \\ & + \alpha(\alpha - 1)\Theta(\theta_d - I_d)[p - \theta_{p0}]^+ . \end{aligned} \quad (22)$$

153 The objective function is shown in Fig. 7. One can observe that states closer to the I_p - I_d diagonal are
 154 preferred, while the opposite is the case for off-diagonal states. This provides an explanation why the
 155 BCM-rule can induce an alignment between proximal and distal inputs when used in combination with the
 156 nonlinear compartment model.

157 It should be noted, though, that to a certain extent, the objective function is not scale-invariant (as would
 158 be e.g. if the squared error was used) in the sense that the prior distributions of both proximal and distal
 159 inputs need a certain mean and variance to cover a region of input states for which the described effects
 160 can take place. As a counterexample, one could imagine that the input samples only covered a flat of \mathcal{L}_p , as
 161 for example in Fig. 7 on the left, leading to a zero average gradient. This is prevented, however, by the
 162 homeostatic processes acting simultaneously on the gains and biases.

4 DISCUSSION

163 We have demonstrated that in a simple supervised learning scheme, the proposed two-compartment transfer
 164 function significantly increases the robustness of the learning process against distracting components in the
 165 proximal input space. This was most prominently found when combined with a BCM-like learning rule.

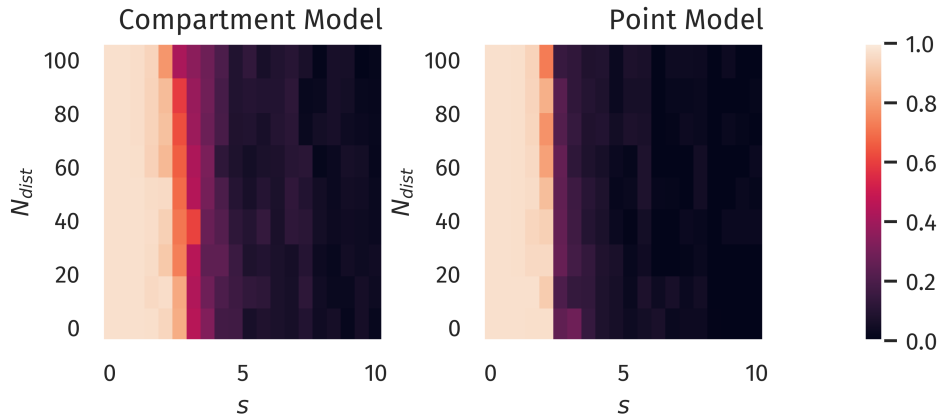


Figure 8. Alignment between Basal and Apical Input after Binary Classification Learning. Correlation between proximal and distal Input after training as described in Sect. 3.2.

166 The idea of target-backpropagation in multi-layered networks has already been proposed in different
 167 variants Bengio (2014); Lee et al. (2015); Guerguiev et al. (2017). Yet, all of these approaches assume
 168 a learning rule being dependent on an explicit error term between top-down and bottom up signals
 169 guiding plasticity in some form or another. In this work, we considered an alternative approach, that
 170 is, the correlation between proximal and distal input as a maximization objective, in combination with
 171 homeostatic adaptation rules that regulate proximal and distal inputs into a desired “working regime”, see
 172 Sect. 3.4. Since I_p is a linear projection of the proximal input space, maximizing the correlation between
 173 I_p and I_d can be regarded as a form of canonical correlation analysis (CCA) Härdle and Simar (2007).
 174 The idea of investigating CCA as a possible mode of synaptic learning has previously been investigated
 175 by Haga and Fukai (2018). Interestingly, according to the authors, a BCM-learning term in the plasticity
 176 dynamics accounts for principal component analysis in the input space, while CCA requires an additional
 177 multiplicative term between local basal and apical activity. In contrast, our results indicate that such a
 178 multiplicative term is not required to drive basal synaptic plasticity towards a maximal alignment between
 179 basal and apical input, even in the presence of distracting principal components.

180 As we did not include higher-dimensional distal input patterns, it remains an open question how target
 181 signals would be formed in multi-layered network structures. However, as previous works have indicated,
 182 random top-down weights can be sufficient for successful credit assignment and learning Lillicrap et al.
 183 (2016); Guerguiev et al. (2017). Therefore, our results could potentially also be transferred to deeper
 184 network structures, where plasticity is guided by local errors between top-down and bottom-up signals.

5 SUPPLEMENTARY MATERIAL

CONFLICT OF INTEREST STATEMENT

185 The authors declare that the research was conducted in the absence of any commercial or financial
 186 relationships that could be construed as a potential conflict of interest.

AUTHOR CONTRIBUTIONS

187 Both authors, F.S. and C.G., contributed equally to the writing and review of the manuscript. F.S. provided
 188 the code, ran the simulations and prepared the figures.

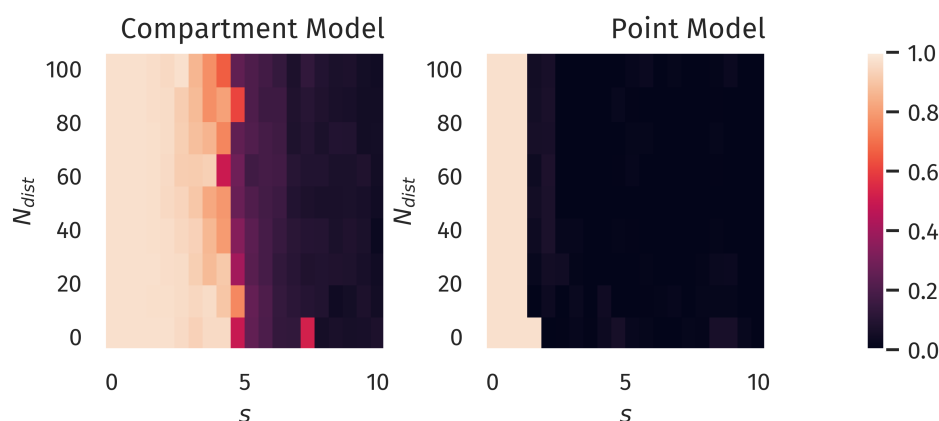


Figure 9. Alignment between Basal and Apical Input after Binary Classification Learning using a BCM-like Rule. Correlation between proximal and distal Input after linear classification training as described in Sect. 3.2, but using the plasticity rules given in Sect. 3.3.

ACKNOWLEDGMENTS

189 The authors acknowledge the financial support of the German research foundation (DFG)

SUPPLEMENTAL DATA

190 Supplementary Material should be uploaded separately on submission, if there are Supplementary Figures,
191 please include the caption in the same file as the figure. LaTeX Supplementary Material templates can be
192 found in the Frontiers LaTeX folder.

DATA AVAILABILITY STATEMENT

193 The datasets [GENERATED/ANALYZED] for this study can be found in the [NAME OF REPOSITORY]
194 [LINK].

REFERENCES

- 195 Bengio, Y. (2014). How Auto-Encoders Could Provide Credit Assignment in Deep Networks via Target
196 Propagation
- 197 Bi, G. Q. and Poo, M. M. (1998). Synaptic modifications in cultured hippocampal neurons: Dependence on
198 spike timing, synaptic strength, and postsynaptic cell type. *Journal of Neuroscience* 18, 10464–10472.
199 doi:10.1523/jneurosci.18-24-10464.1998
- 200 Bienenstock, E. L., Cooper, L. N., and Munro, P. W. (1982). Theory for the development of neuron
201 selectivity: Orientation specificity and binocular interaction in visual cortex. *Journal of Neuroscience* 2,
202 32–48. doi:10.1523/jneurosci.02-01-00032.1982
- 203 Branco, T. and Häusser, M. (2011). Synaptic Integration Gradients in Single Cortical Pyramidal Cell
204 Dendrites. *Neuron* 69, 885–892. doi:10.1016/j.neuron.2011.02.006
- 205 Debanne, D., Gähwiler, B. H., and Thompson, S. M. (1994). Asynchronous pre- and postsynaptic activity
206 induces associative long-term depression in area CA1 of the rat hippocampus in vitro. *Proceedings of*
207 *the National Academy of Sciences of the United States of America* 91, 1148–1152. doi:10.1073/pnas.91.
208 3.1148
- 209 Ebner, C., Clopath, C., Jedlicka, P., and Cuntz, H. (2019). Unifying Long-Term Plasticity Rules for
210 Excitatory Synapses by Modeling Dendrites of Cortical Pyramidal Neurons. *Cell Reports* 29, 4295–
211 4307.e6. doi:10.1016/j.celrep.2019.11.068

- Guerguiev, J., Lillicrap, T. P., and Richards, B. A. (2017). Towards deep learning with segregated dendrites. *eLife* 6. doi:10.7554/eLife.22901
- Gustafsson, B., Wigstrom, H., Abraham, W. C., and Huang, Y. Y. (1987). Long-term potentiation in the hippocampus using depolarizing current pulses as the conditioning stimulus to single volley synaptic potentials. *Journal of Neuroscience* 7, 774–780. doi:10.1523/jneurosci.07-03-00774.1987
- Haga, T. and Fukai, T. (2018). Dendritic processing of spontaneous neuronal sequences for single-trial learning. *Scientific Reports* 8, 15166. doi:10.1038/s41598-018-33513-9
- Härdle, W. and Simar, L. (2007). Canonical Correlation Analysis. In *Applied Multivariate Statistical Analysis* (Berlin, Heidelberg: Springer Berlin Heidelberg). 321–330. doi:10.1007/978-3-540-72244-1_14
- [Dataset] Häusser, M., Spruston, N., and Stuart, G. J. (2000). Diversity and dynamics of dendritic signaling. doi:10.1126/science.290.5492.739
- Hay, E., Hill, S., Schürmann, F., Markram, H., and Segev, I. (2011). Models of Neocortical Layer 5b Pyramidal Cells Capturing a Wide Range of Dendritic and Perisomatic Active Properties. *PLoS Computational Biology* 7, e1002107. doi:10.1371/journal.pcbi.1002107
- Intrator, N. and Cooper, L. N. (1992). Objective function formulation of the BCM theory of visual cortical plasticity: Statistical connections, stability conditions. *Neural Networks* 5, 3–17. doi:10.1016/S0893-6080(05)80003-6
- [Dataset] Larkum, M. (2013). A cellular mechanism for cortical associations: An organizing principle for the cerebral cortex. doi:10.1016/j.tins.2012.11.006
- Larkum, M. E., Nevian, T., Sandier, M., Polsky, A., and Schiller, J. (2009). Synaptic integration in tuft dendrites of layer 5 pyramidal neurons: A new unifying principle. *Science* 325, 756–760. doi:10.1126/science.1171958
- Law, C. C. and Cooper, L. N. (1994). Formation of receptive fields in realistic visual environments according to the Bienenstock, Cooper, and Munro (BCM) theory. *Proceedings of the National Academy of Sciences of the United States of America* 91, 7797–7801. doi:10.1073/pnas.91.16.7797
- Lee, D. H., Zhang, S., Fischer, A., and Bengio, Y. (2015). Difference target propagation. In *Lecture Notes in Computer Science (including subseries Lecture Notes in Artificial Intelligence and Lecture Notes in Bioinformatics)* (Springer Verlag), vol. 9284, 498–515. doi:10.1007/978-3-319-23528-8_31
- Letzkus, J. J., Kampa, B. M., and Stuart, G. J. (2006). Learning Rules for Spike Timing-Dependent Plasticity Depend on Dendritic Synapse Location. *Journal of Neuroscience* 26, 10420–10429. doi:10.1523/JNEUROSCI.2650-06.2006
- Lillicrap, T. P., Cownden, D., Tweed, D. B., and Akerman, C. J. (2016). Random synaptic feedback weights support error backpropagation for deep learning. *Nature Communications* 7, 1–10. doi:10.1038/ncomms13276
- Markram, H., Lübke, J., Frotscher, M., and Sakmann, B. (1997). Regulation of synaptic efficacy by coincidence of postsynaptic APs and EPSPs. *Science* 275, 213–215. doi:10.1126/science.275.5297.213
- Poirazi, P. (2009). Information processing in single cells and small networks: Insights from compartmental models. In *AIP Conference Proceedings* (American Institute of Physics), vol. 1108, 158–167. doi:10.1063/1.3117124
- [Dataset] Ramaswamy, S. and Markram, H. (2015). Anatomy and physiology of the thick-tufted layer 5 pyramidal neuron. doi:10.3389/fncel.2015.00233
- Schiess, M., Urbanczik, R., and Senn, W. (2016). Somato-dendritic Synaptic Plasticity and Error-backpropagation in Active Dendrites. *PLoS Computational Biology* 12, 1004638. doi:10.1371/journal.pcbi.1004638

- 257 Shai, A. S., Anastassiou, C. A., Larkum, M. E., and Koch, C. (2015a). Physiology of Layer 5
258 Pyramidal Neurons in Mouse Primary Visual Cortex: Coincidence Detection through Bursting. *PLOS*
259 *Computational Biology* 11
- 260 Shai, A. S., Anastassiou, C. A., Larkum, M. E., and Koch, C. (2015b). Physiology of Layer 5
261 Pyramidal Neurons in Mouse Primary Visual Cortex: Coincidence Detection through Bursting. *PLOS*
262 *Computational Biology* 11
- 263 Sjöström, P. J. and Häusser, M. (2006). A Cooperative Switch Determines the Sign of Synaptic Plasticity
264 in Distal Dendrites of Neocortical Pyramidal Neurons. *Neuron* 51, 227–238. doi:10.1016/j.neuron.2006.
265 06.017
- 266 Spruston, N. (2008). Pyramidal neurons: dendritic structure and synaptic integration. *Nature Reviews*
267 *Neuroscience* 9, 206–221. doi:10.1038/nrn2286
- 268 Spruston, N., Schiller, Y., Stuart, G., and Sakmann, B. (1995). Activity-dependent action potential invasion
269 and calcium influx into hippocampal CA1 dendrites. *Science* 268, 297–300. doi:10.1126/science.
270 7716524
- 271 Stuart, G. J. and Häusser, M. (2001). Dendritic coincidence detection of EPSPs and action potentials.
272 *Nature Neuroscience* 4, 63–71. doi:10.1038/82910
- 273 Urbanczik, R. and Senn, W. (2014). Learning by the Dendritic Prediction of Somatic Spiking. *Neuron* 81,
274 521–528. doi:10.1016/j.neuron.2013.11.030